PHYSICAL REVIEW C **87**, 034906 (2013)

Flow vorticity in peripheral high-energy heavy-ion collisions

L. P. Csernai,[1] V. K. Magas,[2] and D. J. Wang[1]
[1]*Institute of Physics and Technology, University of Bergen, Allegaten 55, 5007 Bergen, Norway*
[2]*Departament d'Estructura i Constituents de la Matèria, Universitat de Barcelona, 08028 Barcelona, Spain*
(Received 11 November 2012; published 22 March 2013)

Vorticity development is studied in the reaction plane of peripheral relativistic heavy-ion reactions where the initial state has substantial angular momentum. The earlier predicted rotation effect and Kelvin Helmholtz instability lead to significant initial vorticity and circulation. In low-viscosity quark gluon plasma this vorticity remains still significant at the time of freeze-out of the system, even if damping due to explosive expansion and dissipation decreases the vorticity and circulation. In the reaction plane the vorticity arises from the initial angular momentum, and it is stronger than in the transverse plane, where vorticity is caused by random fluctuations only.

DOI: 10.1103/PhysRevC.87.034906 PACS number(s): 12.38.Mh, 25.75.Nq, 25.75.Ld, 24.85.+p

I. INTRODUCTION

The strongly interacting quark gluon plasma (QGP) [1] has raised many interesting questions about the physics of ultra-dense hot matter produced in relativistic heavy-ion collisions. Many transport and hydrodynamic models [2] are popular for analyzing the evolution of the viscous QGP and its properties. In peripheral heavy-ion reactions, due to the initial angular momentum, the initial state of the fluid dynamical stage of the collision dynamics has shear flow characteristics, and this leads to rotation [3] and even Kelvin Helmholtz instability (KHI) [4] in the reaction plane for low-viscosity quark-gluon plasma. This possibility was indicated by high-resolution computational fluid dynamics (CFD) calculations using the Particle in Cell (PIC) method. We study the development of these processes in $(3+1)$-dimensional $(3+1\mathrm{D})$ configuration to describe the energy and momentum balance realistically.

In idealized $2+1\mathrm{D}$ model calculations the dissipation due to 3D expansion is neglected, and thus the dissipation due to the 3D viscous expansion is also neglected, which results in unrealistic estimates. The vorticity of the flow is especially sensitive to such oversimplifications: while in $2+1\mathrm{D}$ the integrated vorticity is conserved in perfect fluid flow, the decrease of vorticity is essential in realistic $3+1\mathrm{D}$ CFD description.

In Ref. [5], the angular momentum is assumed to have significant effects on the longitudinal flow velocity and on its distribution in the transverse plane, so that it gives rise to vorticity and polarization. The arising polarization is also studied in Ref. [6], where a laminar shear flow is assumed with each layer having a different velocity, which is quite similar to the initial-state velocity profile depicted in Fig. 1. This type of initial state is described in great detail in Ref. [7]. In our present fluid dynamical calculation we use this initial-state model, which is tested in several model calculations in the past decade. It describes correctly the initial shear flow characteristics. The initial angular momentum is based on the assumption that the initial angular momentum of the participants (based on straight propagation geometry) is streak by streak conserved. This leads to strong shear flow, as shown in Fig. 2. This model assumes that the incoming Lorentz contracted nuclei interpenetrate each other, and the leading charges in each streak are slowed down by the large string-rope tension. This takes about 3–5 fm/c for heavy nuclei, depending on the impact parameter. Then local equilibration is reached and the fluid dynamical evolution starts.

In this work we study the development of vorticity in high-energy heavy-ion reactions, and the development of the above mentioned specific effects, which may arise in low-viscosity [8,9] QGP.

We also compare the classical vorticity characteristics, and the most dominant relativistic generalizations. These comparisons may provide insight into the possibilities of using this method for precision studies of the transport properties of QGP.

It is also important to mention that the shear flow velocity profile is essential from the point of instability. According to our initial-state description of the fluid dynamical calculations (Fig. 4 of Ref. [4]) the velocity profile along the x axis is not linear but has a $x \sim \tan(v_z)$ shape (dotted line in Fig. 3), which may lead to KHI, in contrast to a $x \sim \arctan(v_z)$ shape, which does not.

In the following we discuss recent approaches to flow vorticity in high-energy heavy-ion collisions and present the vorticity development and its distribution in the reaction plane.

In classical physics for incompressible, perfect fluids vorticity exhibits an impressive conservation law: the conservation of circulation. In high-energy heavy-ion physics the vorticity definition must be modified, and the mentioned idealizations are not applicable to energetic heavy-ion reactions. Still, as CFD calculations indicate typical flow patterns and instabilities may occur here also. Thus their studies can provide insight into the properties of the QGP fluid.

II. THE VORTICITY

A. Classical flow

In the reaction plane, (xz), the vorticity is defined as

$$\omega_y \equiv \omega_{xz} \equiv -\omega_{zx} \equiv \tfrac{1}{2}(\partial_z v_x - \partial_x v_z) \qquad (1)$$

where the x, y, z components of the 3-velocity $\boldsymbol{v}$ are denoted by v_x, v_y, v_z respectively. In this definition we have already included the factor $\frac{1}{2}$ for the symmetrization to have the same

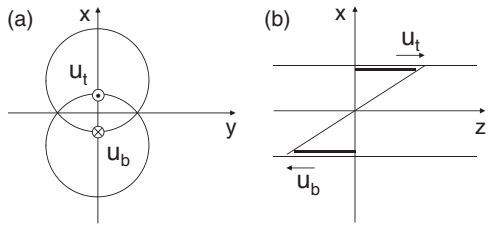

FIG. 1. The sketch of a collision. Panel (a) is in the transverse (xy) plane and (b) is in the reaction (xz) plane. The almond shape in the middle of panel (a) is the participant zone of the event. Right after the collision, streaks are formed, and the top streaks move along the z direction while bottom ones move along the $-z$ direction. This velocity shear may lead to the Kelvin Helmholtz instability, a wave formation, on the interface between the top and bottom sheets.

magnitude of vorticity as for symmetrized volume divergence or expansion rate.

Here we study the vorticity in the reaction plane (in the xz plane), at different times in the CFD development.

In 3-dimensional space the vorticity can be defined as

$$\boldsymbol{\omega} \equiv \tfrac{1}{2}\mathbf{rot}\ \ \boldsymbol{v} = \tfrac{1}{2}\,\nabla \times \boldsymbol{v} \tag{2}$$

(but this cannot be generalized to four or more dimensions). The *circulation* of the flow is the integral of the velocity along a closed curve, C, with the line element $d\boldsymbol{l}$. It is defined as

$$\Gamma = \oint_C \boldsymbol{v}\, d\boldsymbol{l} = \int_A 2\boldsymbol{\omega}\, d\boldsymbol{A},$$

where A is an (arbitrary) surface surrounded by the curve C, and the normal of its surface element is $d\boldsymbol{A}$. For rotationless (potential) flow the circulation vanishes. In peripheral heavy-ion reactions the flow is rotational. In classical fluid dynamics

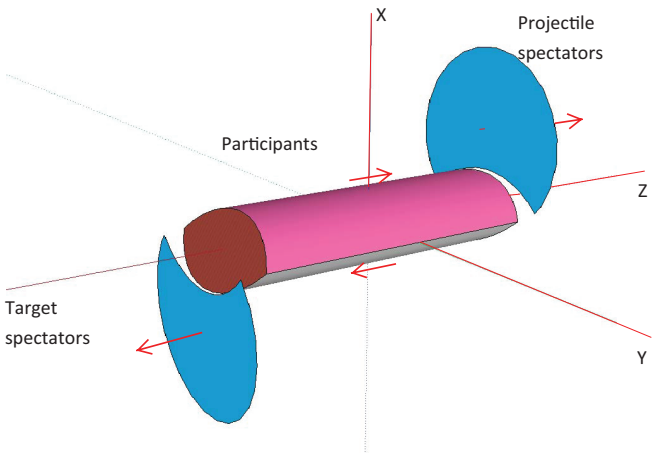

FIG. 2. (Color online) The three-dimensional view of the collision shortly after the impact corresponding to the situation illustrated in Fig. 1(a). The projectile spectators are going along the z direction; and the target spectators are going along the $-z$ axis. We assume that the participants in the middle form a cylinder with an almond-shaped profile and tilted end surfaces, where the top side is moving to the right and the bottom is moving to the left. The participant cylinder can be divided into streaks, and each streak has its own velocity, as shown in Fig. 1(b). The velocity differences among the streaks result in the KHI effect.

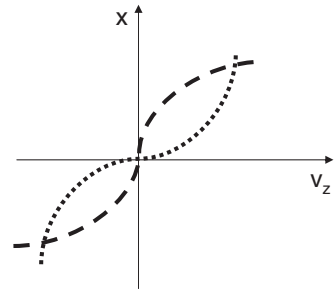

FIG. 3. The velocity along the z axis, v_z, represented by the dotted curve is calculated in our CFD model and presented in Fig. 4 of Ref. [4]. Here we mention that the velocity of the dotted curve will induce the KHI effect, while the dashed curve will not; see Chap. 8 of Ref. [10].

the circulation is constant in a fluid along the line of motion of a fluid element if the viscosity of the flow vanishes and flow is barotropic; i.e., the pressure depends only on the density of the fluid, $P = P(\rho)$. These conditions are not satisfied for QGP in heavy-ion reactions.

In the relativistic case the formulation of fluid dynamics is more involved, and the formalism must be modified [11,12]. The 3-velocities are replaced by 4-velocities, the derivatives should take into account the world lines of the particles and the changes of these with time, and the mass density is replaced by the energy density where the pressure will have a non-negligible role. This last modification leads to a modified relativistic definition of the vorticity and circulation, which includes the specific enthalpy of the fluid [13]. This would then extend the validity of the conservation of circulation under the same conditions. On the other hand, this modified relativistic vorticity would then have a different dimension and it would not be conserved anyway in heavy-ion reactions where the conditions of validity are not satisfied.

Thus, in the present work we intend to keep the possibility of comparison to the classical vorticity and circulation; in a relativistic system where the (baryon charge) density and temperature change violently, the pressure is not negligible and does not depend on the density only. Still the energy and momentum (T^{00} and T^{i0}) are strictly conserved, and the total energy remains constant while the momentum vanishes (in the c.m. frame).

Keeping in view fluid dynamics with fluid elements, we introduce a weight proportional to the energy content of the fluid element. The energy distribution (and thus the local angular momentum) of the matter is highly nonhomogeneous in a heavy-ion reaction. To reflect our physical situation better, we weight the contribution of our fluid cells by the local energy density in the reaction plane, however, without changing the average vorticity in the layer of the reaction plane. Thus we weight with a distribution normalized to unity. We define an energy-density-weighted, average vorticity as

$$\Omega_{zx} \equiv w(z,x)\omega_{zx} \tag{3}$$

so that this weighting does not change the average circulation of the layer, i.e., the sum of the average of the weights over all fluid cells is unity, $\langle w(z,x)\rangle = 1$, both if we consider one y layer only or if we consider all y layers. This weighting does

not change the average vorticity value of the set; just the cells will have larger weight with more energy content, T^{00}.

As we have discretized fluid cells, we study separately the reaction plane, one y layer, or the whole system, all y layers. The total energy content of a cell at point (z, x) or the corresponding i, k is $E_{ik} = T^{00}(z, x)$. The total energy in a y layer (or in all y layers) is $E_{\rm tot} = \sum_{ik} E_{ik}$, while the number of the cells in a y layer (or in all y layers) is $N_{\rm cell}$. Thus the average energy for for a fluid cell is $E_{\rm tot}/N_{\rm cell}$ in both cases. We divide the actual energy of a fluid cell, E_{ik}, with the average fluid cell energy $E_{\rm tot}/N_{\rm cell}$, so that the vorticity values on average will remain comparable with the nonweighted values, but still larger energy cells will have more weight. The total energy $\sum_{\rm All\ cells} T^{00}$ remains exactly constant in our case (in the numerical calculation to 10^{-16} accuracy). Of course this is not true for a single layer like the reaction plane.

Our weight, then, should be proportional with the local energy density

$$w_{ik} \equiv \frac{E_{ik}}{(E_{\rm tot}/N_{\rm cell})}.$$

Within the reaction plane, at a given moment of time, the cells carrying larger amounts of energy will get larger weights than those carrying less energy. The edge cells, carrying less energy, show stronger fluctuations.

This average vorticity weighted by the cell energy, which is a conserved quantity for all cells, provides the possibility of comparing the results to classical systems and their features.

An alternative method to present the relativistic vorticity, as in Ref. [13], by weighting with the specific enthalpy, which would provide conserved circulation, Γ, if the pressure were exclusively density dependent. As mentioned earlier, this is

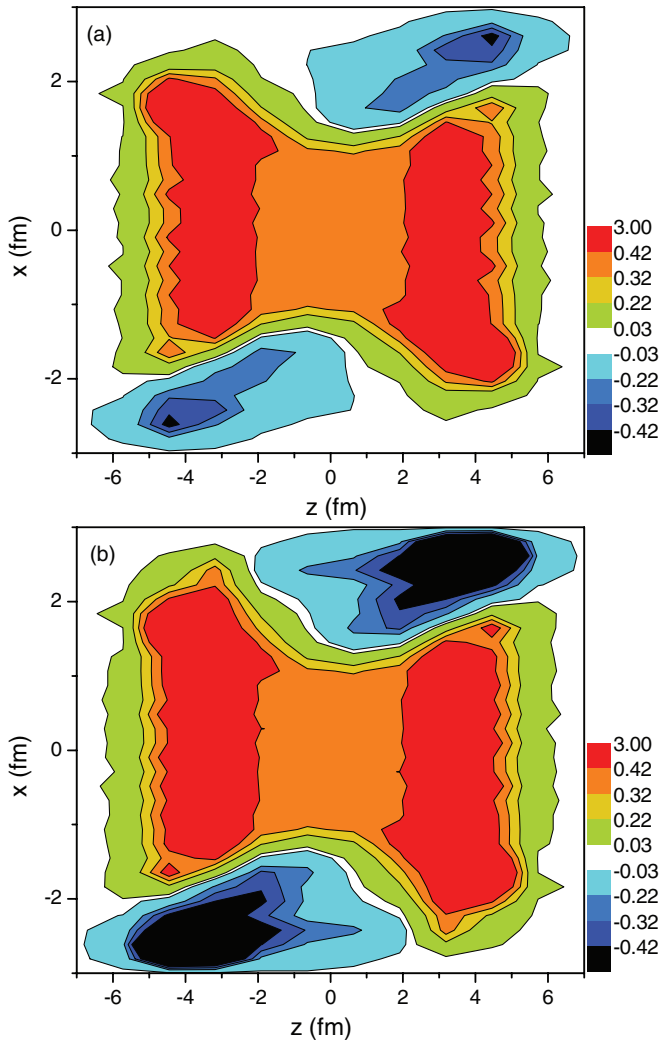

FIG. 4. (Color online) The classical (a) and relativistic (b) weighted vorticity, Ω_{zx} in units of c/fm, calculated in the reaction (xz) plane at $t = 0.17$ fm/c after the start of fluid dynamical evolution. The collision energy is $\sqrt{s_{NN}} = 2.76$ TeV and $b = 0.7\, b_{\rm max}$, the cell size is $dx = dy = dz = 0.4375$ fm. The average vorticity in the reaction plane is 0.1434 (0.1185) c/fm for the classical (relativistic) weighted vorticities respectively.

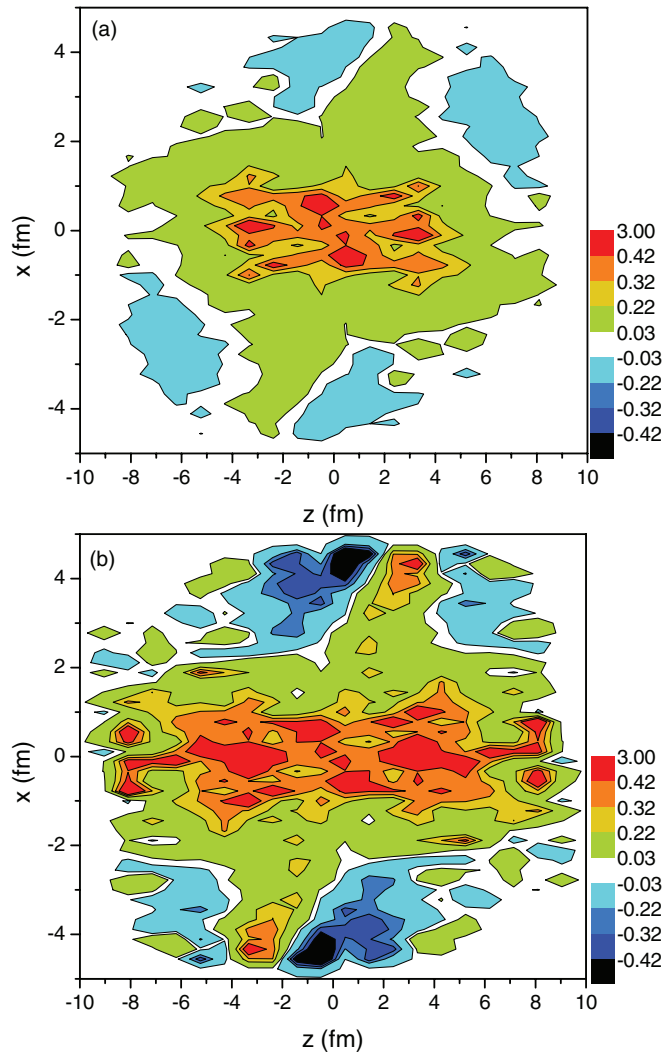

FIG. 5. (Color online) The classical (a) and relativistic (b) weighted vorticity, Ω_{zx} (c/fm), calculated in the reaction xz plane at $t = 3.56$ fm/c. The collision energy is $\sqrt{s_{NN}} = 2.76$ TeV and $b = 0.7\, b_{\rm max}$, and the cell size is $dx = dy = dz = 0.4375$ fm. The average vorticity in the reaction plane is 0.04845 (0.07937) c/fm for the classical (relativistic) weighted vorticity respectively.

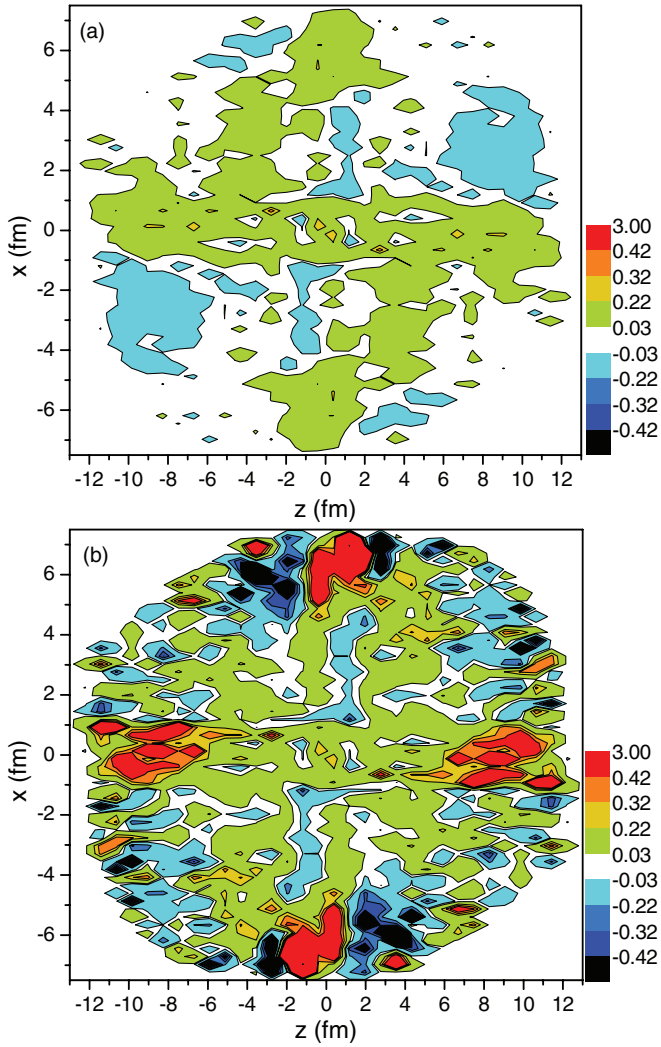

FIG. 6. (Color online) The classical (a) and relativistic (b) weighted vorticity Ω_{zx} (c/fm), calculated in the reaction xz plane at $t = 6.94$ fm/c. The collision energy is $\sqrt{s_{NN}} = 2.76$ TeV and $b = 0.7\, b_{\max}$; the cell size is $dx = dy = dz = 0.4375$ fm. The average vorticity in the reaction plane is 0.01555 (0.05881) c/fm for the classical (relativistic) weighted vorticity respectively.

not the case for QGP, so for us this advantage is not realized, while this weighting changes both the value and the dimension of the vorticity, so it would make the comparison to classical results difficult.

The weighted vorticities in the reaction xz plane at different time steps are shown in the Figs. 4–6.

B. Relativistic flow

We are following the definition in Ref. [12] for the relativistic case. The expansion rate Θ and the vorticity tensor ω^{μ}_{ν} are defined as

$$\Theta \equiv \nabla_{\mu} u^{\mu} = \partial_{\mu} u^{\mu}, \tag{4}$$

$$\omega^{\mu}_{\nu} \equiv \tfrac{1}{2}(\nabla_{\nu} u^{\mu} - \nabla^{\mu} u_{\nu}), \tag{5}$$

where for any 4-vector q^{μ} the quantity $\nabla_{\alpha} q^{\mu} \equiv \Delta^{\beta}_{\alpha}\, \partial_{\beta} q^{\mu} = \Delta^{\beta}_{\alpha}\, q^{\mu}_{,\beta}$ and $\Delta^{\mu\nu} \equiv g^{\mu\nu} - u^{\mu} u^{\nu}$. This leads to

$$\begin{aligned}\omega^{\mu}_{\nu} &= \tfrac{1}{2}\Delta^{\mu\alpha}\Delta^{\beta}_{\nu}(u_{\alpha,\beta} - u_{\beta,\alpha}) \\ &= \tfrac{1}{2}[(\partial_{\nu} u^{\mu} - \partial^{\mu} u_{\nu}) + (u^{\mu} u^{\alpha}\partial_{\alpha} u_{\nu} - u_{\nu} u^{\alpha}\partial_{\alpha} u^{\mu})] \\ &= \tfrac{1}{2}[(\partial_{\nu} u^{\mu} - \partial^{\mu} u_{\nu}) + (u^{\mu}\partial_{\tau} u_{\nu} - u_{\nu}\partial_{\tau} u^{\mu})],\end{aligned}$$

where $\partial_{\tau} u^{\mu} \equiv \dot{u}^{\mu} = u^{\alpha}\partial_{\alpha} u^{\mu}$ is the proper time derivative of u^{μ}.

In our initial state in the middle part of the collision the streaks are stopped after two Lorentz contracted ions collide and interpenetrate each other. If the acceleration of the fluid elements is negligible compared to the rotation, $|\partial_{\tau} u^{\mu}| \ll |\partial_{x} u^{z}|$, this assumption holds for the initial moments in our model, which has strong initial shear flow. Thus the second term can be dropped. This is also the case considered in Ref. [11], while studying the vorticity in the xy plane instead of the reaction plane. In this case the relativistic vorticity is

$$\omega_{\mu\nu} = \tfrac{1}{2}(\partial_{\nu} u_{\mu} - \partial_{\mu} u_{\nu}) \tag{6}$$

where

$$\partial^{\nu} = (\partial_0, \partial_x, \partial_y, \partial_z), \quad u_{\mu} = \gamma(1, -v_x, -v_y, -v_z).$$

Let us expand Eq. (6) in four dimensions:

$$\omega^{\nu}_{\mu} = \frac{1}{2}\left[\begin{pmatrix} \partial_0\gamma & -\partial_0\gamma v_x & -\partial_0\gamma v_y & -\partial_0\gamma v_z \\ \partial_x\gamma & -\partial_x\gamma v_x & -\partial_x\gamma v_y & -\partial_x\gamma v_z \\ \partial_y\gamma & -\partial_y\gamma v_x & -\partial_y\gamma v_y & -\partial_y\gamma v_z \\ \partial_z\gamma & -\partial_z\gamma v_x & -\partial_z\gamma v_y & -\partial_z\gamma v_z \end{pmatrix} - \begin{pmatrix} \partial_0\gamma & \partial_x\gamma & \partial_y\gamma & \partial_z\gamma \\ -\partial_0\gamma v_x & -\partial_x\gamma v_x & -\partial_y\gamma v_x & -\partial_z\gamma v_x \\ -\partial_0\gamma v_y & -\partial_x\gamma v_y & -\partial_y\gamma v_y & -\partial_z\gamma v_y \\ -\partial_0\gamma v_z & -\partial_x\gamma v_z & -\partial_y\gamma v_z & -\partial_z\gamma v_z \end{pmatrix}\right], \tag{7}$$

and we see that the vorticity is an antisymmetric tensor. Here for the vorticity development in the reaction plane we calculate ω_{24}:

$$\begin{aligned}\omega^{x}_{z} &= -\omega^{z}_{x} = \tfrac{1}{2}(\partial_z\gamma v_x - \partial_x\gamma v_z) \\ &= \tfrac{1}{2}\gamma(\partial_z v_x - \partial_x v_z) + \tfrac{1}{2}(v_x\partial_z\gamma - v_z\partial_x\gamma).\end{aligned} \tag{8}$$

The fluid cells are weighted the same way as in the nonrelativistic vorticity estimate. Due to the fact that the relativistic vorticity includes the relativistic γ factor, Eq. (8), the vorticity increases, especially at the edges where the cells have larger flow velocities.

The weighted relativistic vorticity distributions in the reaction xz plane at different time steps are shown in the Figs. 4–6. At the last time step presented, in the reaction plane we have already an extended area occupied with matter. In case of peripheral reactions the multiplicity is already small, and thus the fluctuations in the reaction plane are considerable. In the relativistic case the outside edges show larger vorticity and the random fluctuations are still strong.

III. WEIGHTED VORTICITY DISTRIBUTIONS

The relativistic vorticity distributions have increased amplitudes compared to the classic ones, due to the relativistic γ factor and its derivatives in the relativistic expression. This is especially visible at the edges where the flow velocities are the largest.

The amplitude of weighted vorticity decreases with time as the matter expands. Random fluctuations are apparent at late times for the dilute matter, especially at the edges, and particularly for the relativistic vorticity, which has enhanced amplitudes.

With increasing time the fluid expands, and outside a more dense shell develops with a less dense central zone. This feature is also apparent in the vorticity distribution of the mater in the central reaction plane, where the central part has smaller weighted vorticity amplitude.

The noncentral, parallel layers, at increasing y values, have similar positive weighted vortices, $\Omega_{zx}^{y_i}$. These outside layers have steeper boundaries in the x direction, which fall into the outside zone of the expanding matter.

We can average the weighted vorticity distributions over all layers parallel to the reaction plane. This compensates for the low-density central zone in the reaction plane and leads to a more uniform, layer-averaged distribution, with higher positive peak amplitudes and smaller negative values. The last presented time step at around $t = 7$ fm/c is still strongly fluctuating for the relativistic case. The weighted vorticity averaged over all layers parallel to the reaction xz plane at different time steps are shown in Figs. 7–9. The dominant effect of the relativistic treatment is visible the most in Fig. 9. By comparing Eqs. (2) and (8), the role of the relativistic γ factor is apparent. As discussed after Eq. (8), the large peripheral velocities make the vorticity large at the external

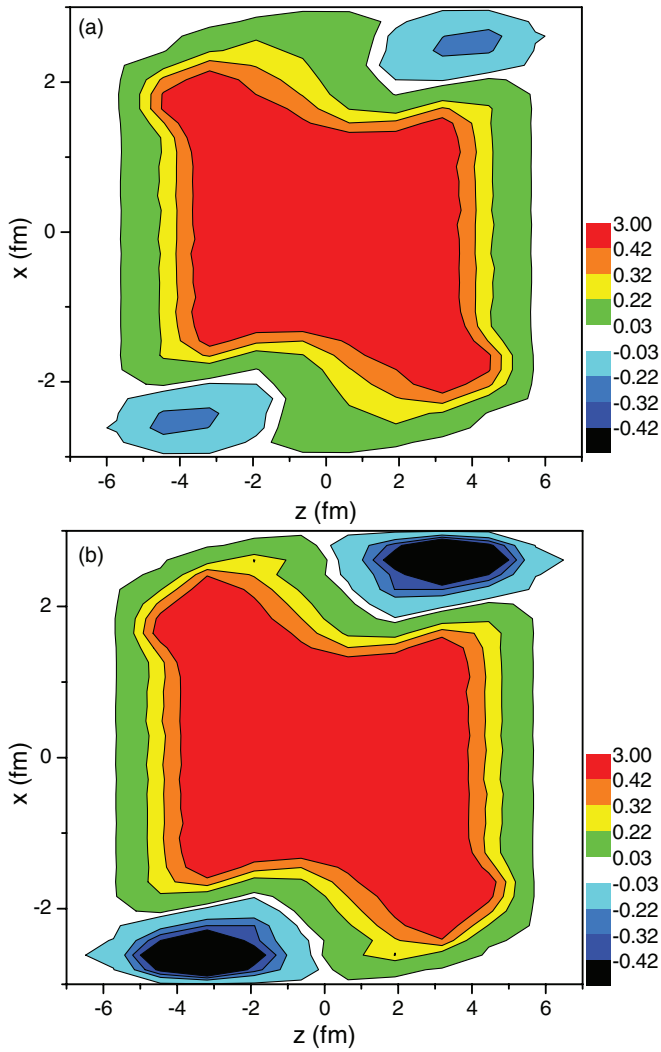

FIG. 7. (Color online) The classical (a) and relativistic (b) weighted vorticity calculated for all xz layers at $t = 0.17$ fm/c. The collision energy is $\sqrt{s_{NN}} = 2.76$ TeV and $b = 0.7\, b_{\max}$, the cell size is $dx = dy = dz = 0.4375$ fm. The average vorticity in the reaction plane is 0.1971 (0.19004) c/fm for the classical (relativistic) weighted vorticity respectively.

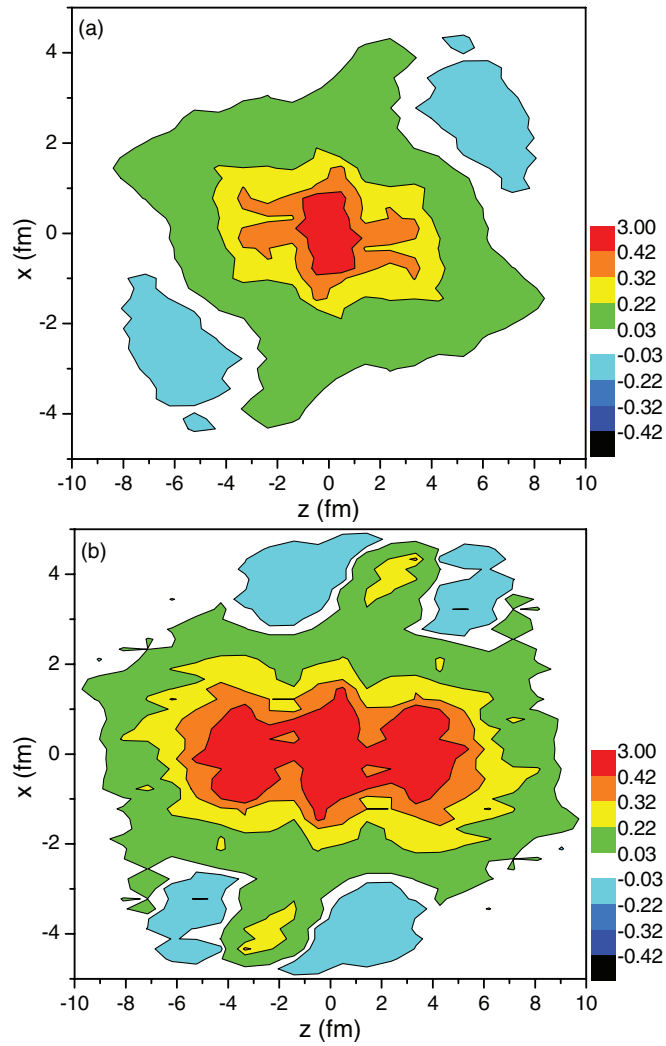

FIG. 8. (Color online) The classical (a) and relativistic (b) weighted vorticity calculated for all xz layers at $t = 3.56$ fm/c. The collision energy is $\sqrt{s_{NN}} = 2.76$ TeV and $b = 0.7\, b_{\max}$, and the cell size is $dx = dy = dz = 0.4375$ fm. The average vorticity in the reaction plane is 0.0538 (0.10685) c/fm for the classical (relativistic) weighted vorticity respectively.

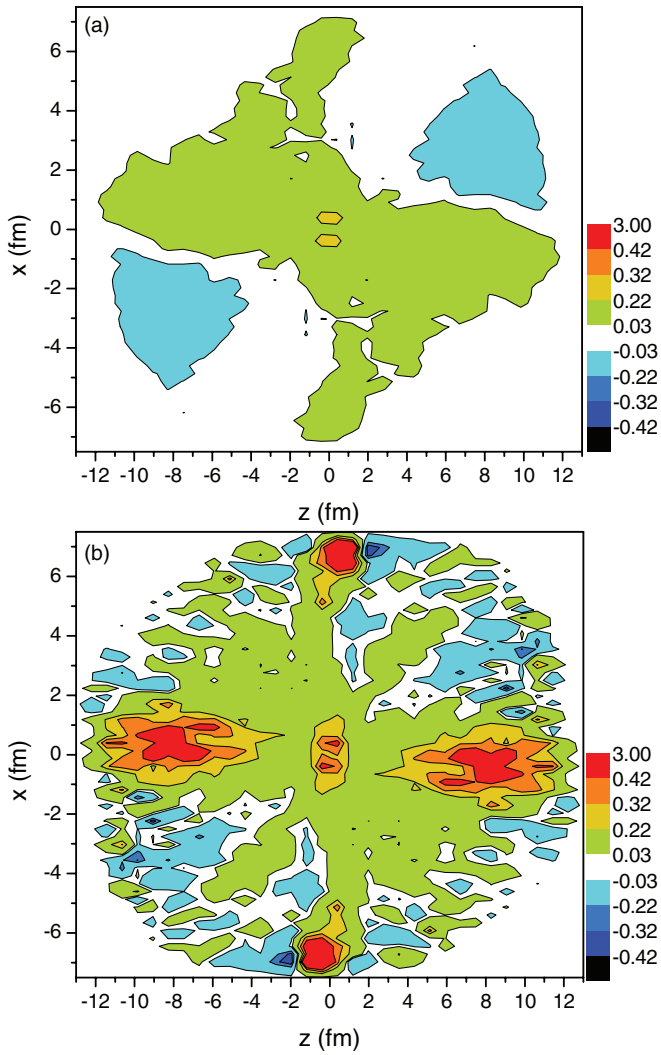

FIG. 9. (Color online) The classical (a) and relativistic (b) weighted vorticity calculated for all xz layers at $t = 6.94$ fm/c. The collision energy is $\sqrt{s_{NN}} = 2.76$ TeV and $b = 0.7\, b_{\max}$, and the cell size is $dx = dy = dz = 0.4375$ fm. The average vorticity in the reaction plane is 0.0159 (0.05881) c/fm for the classical (relativistic) weighted vorticity respectively.

surfaces of the expanding system. At these external regions the matter density is small and the relative density fluctuations are large, so the fluctuations of the surface region vorticities are large.

IV. THE PROPERTIES OF VORTICITY AND CIRCULATION

In Sec. II we introduced the classical vorticity and circulation with the conservation laws for the circulation in case of certain conditions. These can be extended to the relativistic case if we define the relativistic circulation [13] (Chap. 14.3) as

$$\Gamma(C) = \frac{1}{m} \oint_C w\, u^\mu \delta x_\mu,$$

where the weight, w, is the specific enthalpy, $e + P$, over the baryon number, n, and m is the effective mass per net baryon. Applying the Euler equation for perfect fluids results in

$$\frac{\partial \Gamma(C)}{\partial \tau} = \frac{1}{m} \oint_C \frac{\partial^\nu P}{n} \delta x_\nu + \frac{1}{m} \oint_C w\, u^\mu \delta u_\mu, \qquad (9)$$

where the last term vanishes along the flow stream line because $u^\mu \delta u_\mu = 0$. Thus, if the pressure P depends on the density n, only the second term for a closed loop integral also disappears, and the circulation remains constant just as in the classical case.

In our problem these conditions are not satisfied, so we used the same weighting as in the classical case and evaluated the circulation with the weighting as in the classical case to enable the comparison; see Fig. 10. We performed the integral over the xz surface for the weighted relativistic vorticities averaged over all y layers.

Let us take the surface area of the reaction plane, which is filled with fluid, and take the bounding curve at the outside edges of the fluid in this plane. This curve expands with the fluid. In our case in rapidly expanding and nonperfect fluid the circulation as well as the vorticity in the xz reaction plane are both decreasing.

For us the rate of this decrease is important to see if we can still detect the vorticity and circulation at freeze-out. Notice that we calculated only the Ω_{zx} component of the weighted vorticity distributions. Due to the close to spherical expansion, the direction of vorticity may develop into different directions. This also contributes to the decrease of the circulation.

We calculated and presented the weighted vorticity distribution in the reaction plane, calculated it for all the xz layers at different y values, and took the average of these vorticity distributions; see Figs. 7–9, 11(b), and 12(b). The overall vorticity is positive, this originates from the initial shear flow configuration. It decreases with time, not only because the weight of the reaction plane decreases due to the expansion but also because of the viscous dissipation in the 3D expansion.

The examples above are for the configuration where the KHI is predicted to occur in heavy-ion collisions at the Large Hadron Collider (LHC).

We also studied how the vorticity and circulation change with increased (numerical) viscosity and for more central collisions, where the occurrence of KHI is not predicted by the CFD model; see Figs. 11(a) and 12(a).

In Ref. [4] it was suggested that the KHI leads to an increased $v_1(y)$ peak. We search for other, preferably more sensitive and more specific experimental methods to identify rotation and KHI and possibly also to separate the two effects.

The vorticity is also strikingly different for the configurations which are adequate for KHI and for those which not, and show only rotation. The initial and intermediate time stages are compared for two different configurations where KHI may and may not appear.

The primary reason of the difference with KHI is that in the highly peripheral reactions the profile height is smaller but the asymmetry between the target and projectile contributions is larger at the edges, and thus the shear in the matter is considerably larger. Consequently both the maximum value of vorticity and the average are larger for the more peripheral configuration: The initial average vorticity is almost three times larger in the more peripheral configuration favorable for KHI than in the less favorable one.

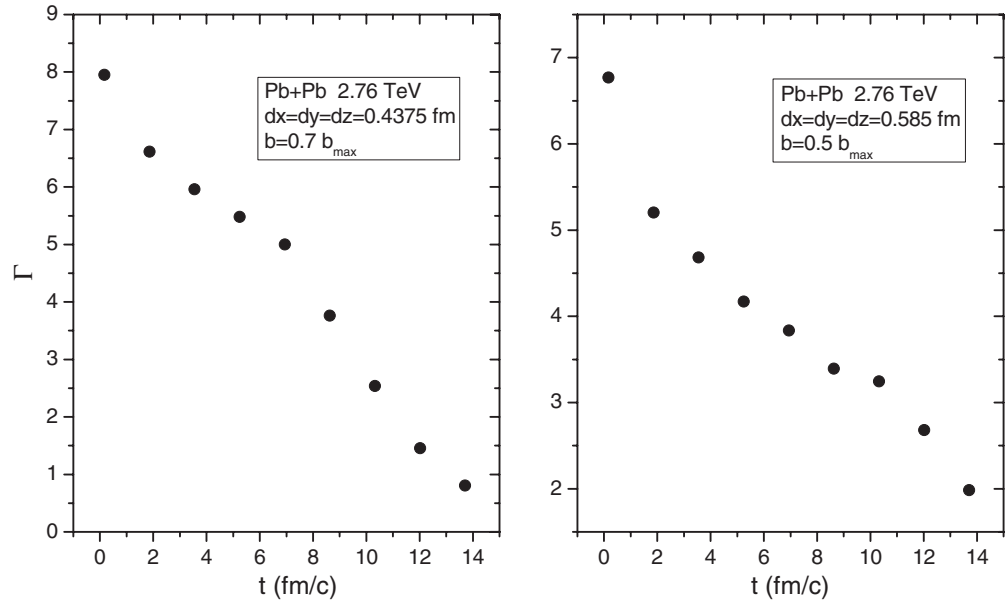

FIG. 10. The time dependence of classical circulation, $\Gamma(t)$, in units of (fm c), calculated for all xz layers and then taking the average of the circulations for all layers. The collision energy is $\sqrt{s_{NN}} = 2.76$ TeV and $b = 0.7\, b_{\max}$, and the cell size is $dx = dy = dz = 0.4375$ fm (left). For comparison another initial-state configuration was also tested for the same collision energy with $b = 0.5\, b_{\max}$; the cell size is $dx = dy = dz = 0.585$ fm (right). This configuration shows also the rotation, but due to its less favorable parameters it does not show the KHI. Although at this impact parameter, which is less peripheral, the reaction plane has a larger area filled with matter, the initial classical circulation nevertheless is less by about 15%. For the more peripheral case with smaller numerical viscosity the circulation decreases with time faster and the circulation for the two cases becomes equal around $t = 8$–10 fm/c.

At the later time, $t = 3.56$ fm/c, the difference is still large, and the KHI formation leads to a vorticity, which is larger by about a factor of two; see Fig. 12.

This, strong dependence on impact parameter arising in low-viscosity matter is very promising from the point of view of the observability of the effect.

The possibility for observation mentioned in Ref. [4], by the position of the rotated $v_1(y)$ peak, is also visible in Fig. 12, where the vorticity peak position is seen in the two configurations. This peak position may be coupled to the peak position of the earlier mentioned v_1 peak. Here in the configuration favorable for KHI the forward rotation angle of the peak is 37°, while in the less favorable configuration it is 33°. Thus, the KHI arising only in low-viscosity matter leads to a special increase in the rotation and vorticity. The observability via finding the motion of the collective (y-odd) $v_1(y)$ peak is not easy in present LHC experiments because the initial-state fluctuations contribute to large longitudinal c.m. fluctuations, apart from azimuthal fluctuations in the transverse plane [3].

V. CONCLUSIONS

An analysis of the vorticity and circulation development is performed for peripheral Pb + Pb reactions at the CERN LHC energy of $\sqrt{s_{NN}} = 2.76$ TeV. The initial peak vorticity is more than 10 times larger (exceeding 3 c/fm) than the one obtained from random fluctuations in the transverse plane, about 0.2 c/fm [11]. The reason is in the high initial angular momentum arising from the beam energy in noncentral collisions.

Although the vorticity and circulation decrease rapidly due to the explosive expansion of the system, still at 4 fm/c after the beginning of fluid dynamical expansion the peak vorticity is above 3 c/fm in favorable configurations with KHI development and it reaches up to 1 c/fm at the same time for less favorable configurations.

This makes it promising to observe the consequences of this rotation and its sensitivity to turbulent configurations. Not only does the peak vorticity exceed earlier estimates from random fluctuations, but also the predicted average vorticity is substantial; it reaches 0.2 c/fm at favorable initial configurations with KHI, while the average vorticity originating from random fluctuations is vanishing [11,14]. The estimated angular deflection arising from this random origin "chiral vortaic effect" (CVE) [14] is small: $\cos(\delta\phi) \sim 10^{-5}$. The effect arising from the initial angular momentum of a peripheral collision is bigger. This improves the observability of the average vorticity compared to CME and CVE predictions.

In this work we repeat the earlier mentioned observable signatures related to the (rapidity odd component) of the directed, v_1 flow, which is a promising possibility for the observations [15]. The time sequences of the results show that the maximum of vorticity in the side regions rotates; with time it moves forward on the top and the maximum reaches the positive z side for the latest times presented. The even flow harmonics are much less sensitive to this change. The rapidity width of the $v_2(y)$ may be effected weakly. Other methods in different correlation observables are more directly connected to rotation in the flow and will be addressed in forthcoming publications (e.g., Ref. [16]).

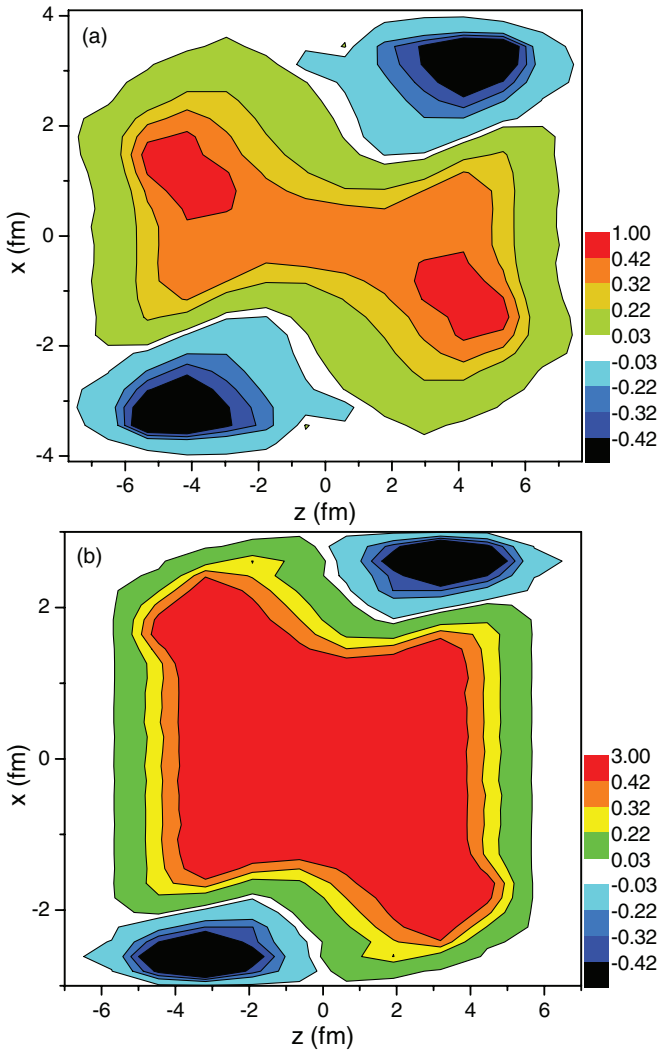

FIG. 11. (Color online) The weighted relativistic vorticity calculated for all xz layers at $t = 0.17$ fm/c. The collision energy is $\sqrt{s_{NN}} = 2.76$ TeV, $b = 0.5\, b_{\max}$ for panel (a) and $b = 0.7\, b_{\max}$ for panel (b). Configuration (a) does not favor KHI while configuration (b) does. The cell size is $dx = dy = dz = 0.585/0.4375$ fm. The average weighted vorticity in the reaction plane is 0.07241/0.19004 c/fm for the two cases respectively. Notice the different color coding scales for panels (a) and (b).

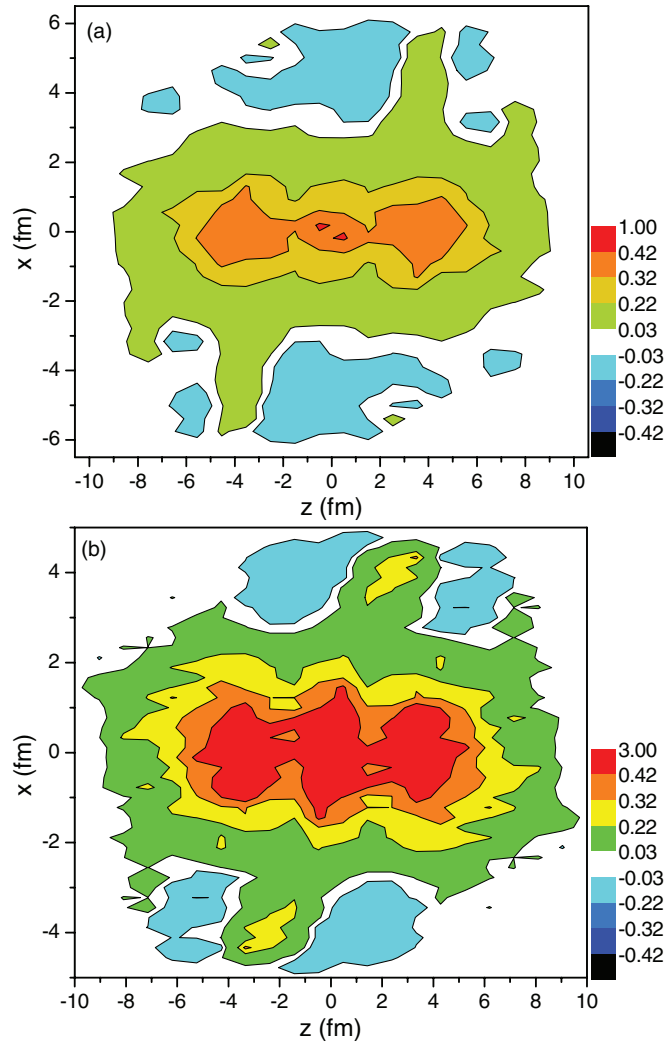

FIG. 12. (Color online) The weighted relativistic vorticity calculated for all xz layers at $t = 3.56$ fm/c. The collision energy is $\sqrt{s_{NN}} = 2.76$ TeV, $b = 0.5\, b_{\max}$ for panel (a) and $b = 0.7\, b_{\max}$ for panel (b). Configuration (a) does not favoring KHI while configuration (b) does. The cell size is $dx = dy = dz = 0.585/0.4375$ fm. The average vorticity in the reaction plane is 0.05242 and 0.10685 c/fm for the two weighted vorticities respectively. Notice the different color scales.

The question arises of how the surface energy influences the rotation and the KHI. The external surface of the expanding QGP is significant, as in the interior the quark gluon fluid has weak interaction (asymptotic freedom) and small viscosity. However, the surface energy has the strongest effect on the hadronization of QGP as first described in Ref. [17]. On the other hand, the collective flow as well as the KHI develops primarily in the early QGP phase as the approximate quark number scaling indicates. At RHIC and LHC energies at this early stage, the surface energy is negligible compared to the energy of the collective flow, and it primarily hinders the early emission of low-energy hadrons from the plasma but does not hinder the rotation. In the KHI the situation is more involved. In the cases where the KHI develops between two fluids (e.g., water-air or oil-air) the large surface tension (e.g., between oil and air) can hinder the development of KHI, as has been well known to sailors for centuries. If the KHI develops within one fluid (like in air or QGP), due to the large shear between the two fluid layers, there is no surface tension in the conventional sense, but the layer with the high shear may have extra energy and can lead to an effective surface tension, which can weaken the development of KHI. See estimates in Ref. [18].

ACKNOWLEDGMENTS

Enlightening discussions with Elena Bratkovskaya and Francesco Becattini are gratefully acknowledged. L.P.C. and D.J.W. thanks for kind hospitality and discussions at the Frankfurt Institute for Advanced Studies.

[1] M. Gyulassy and L. McLerran, Nucl. Phys. A **750**, 30 (2005).
[2] K. Dusling and D. Teaney, Phys. Rev. C **77**, 034905 (2008); D. Molnar and P. Huovinen, J. Phys. G **35**, 104125 (2008).
[3] L. P. Csernai, V. K. Magas, H. Stöcker, and D. D. Strottman, Phys. Rev. C **84**, 024914 (2011).
[4] L. P. Csernai, D. D. Strottman, and C. Anderlik, Phys. Rev. C **85**, 054901 (2012).
[5] F. Becattini, F. Piccinini, and J. Rizzo, Phys. Rev. C **77**, 024906 (2008).
[6] X. G. Huang, P. Huovinen, and X. N. Wang, Phys. Rev. C **84**, 054910 (2011).
[7] V. K. Magas, L. P. Csernai, and D. D. Strottman, Phys. Rev. C **64**, 014901 (2001); Nucl. Phys. A **712**, 167 (2002).
[8] P. K. Kovtun, D. T. Son, and A. O. Starinets, Phys. Rev. Lett. **94**, 111601 (2005).
[9] L. P. Csernai, J. I. Kapusta, and L. D. McLerran, Phys. Rev. Lett. **97**, 152303 (2006).
[10] P. G. Darzin, *Introduction to Hydrodynamic Stability* (Cambridge, Cambridge University Press, 2002).
[11] S. Floerchinger and U. A. Wiedemann, J. High Energy Phys. 11(2011)100; J. Phys. G **38**, 124171 (2011).
[12] E. Molnar, H. Niemi, and D. H. Rischke, Eur. Phys. J. C **65**, 615 (2010).
[13] W. Florkowski, *Phenomenology of Ultra-relativistic Heavy-Ion Collisions* (World Scientific, Singapore, 2010).
[14] O. V. Teryaev, Phys. Atomic Nuclei **75**, 748 (2012); O. V. Rogachevsky, A. S. Sorin, and O. V. Teryaev, Phys. Rev. C **82**, 054910 (2010).
[15] L. P. Csernai, G. Eyyubova, and V. K. Magas, Phys. Rev. C **86**, 024912 (2012).
[16] L. P. Csernai and S. Velle, "Differential Hanbury-Brown–Twiss method to analyze rotation", submitted to Phys. Rev. C.
[17] L. P. Csernai and J. I. Kapusta, Phys. Rev. Lett. **69**, 737 (1992); Phys. Rev. D **46**, 1379 (1992).
[18] D. J. Wang, Z. Néda, and L. P. Csernai, Phys. Rev. C **87**, 024908 (2013).